THE JOURNAL OF PHYSICAL CHEMISTRY B

Article

pubs.acs.org/JPCB

Photoinduced Intra- and Intermolecular Energy Transfer in Chlorophyll *a* Dimer

Fulu Zheng,[†] Sebastian Fernandez-Alberti,[*,‡] Sergei Tretiak,[‖,§] and Yang Zhao[*,†]

[†]Division of Materials Science, Nanyang Technological University, Singapore 639798, Singapore

[‡]Universidad Nacional de Quilmes/CONICET, Roque Saenz Peña 352, B1876BXD Bernal, Argentina

[‖]Theoretical Division, Center for Nonlinear Studies (CNLS), and [§]Center for Integrated Nanotechnologies (CINT), Los Alamos National Laboratory, Los Alamos, New Mexico 87545, United States

ABSTRACT: Applying nonadiabatic excited-state molecular dynamics, we investigate excitation energy transfer and exciton localization dynamics in a chlorophyll *a* (Chl*a*) dimer system at the interface of two monomers of light-harvesting complex II trimer. After its optical excitation at the red edge of the Soret (B) band, the Chl*a* dimer experiences an ultrafast intra- and intermolecular nonradiative relaxation process to the lowest band (Q_y). The energy relaxation is found to run faster in the Chl*a* dimer than in the Chl*a* monomer. Once the molecular system reaches the lowest Q_y band composed of two lowest excited states S_1 and S_2, the concluding relaxation step involves the $S_2 \rightarrow S_1$ population transfer, resulting in a relatively slower relaxation rate. The strength of thermal fluctuations exceeds intraband electronic coupling between the states belonging to a certain band (B, Q_x, and Q_y), producing localized states on individual chromophores. Therefore, time evolution of spatial electronic localization during internal conversion reveals transient trapping on one of the Chl*a* monomers participating in the events of intermonomeric energy exchange. In the phase space domains where electronic states are strongly coupled, these states become nearly degenerate promoting Frenkel-exciton-like delocalization and interchromophore energy transfer. As energy relaxation occurs, redistribution of the transition density on two Chl*a* monomers leads to nearly equal distribution of the exciton among the molecules. For a single Chl*a*, our analysis of excitonic dynamics reveals wave function amplitude transfer from nitrogen and outer carbon atoms to inner carbon atoms during nonradiative relaxation.

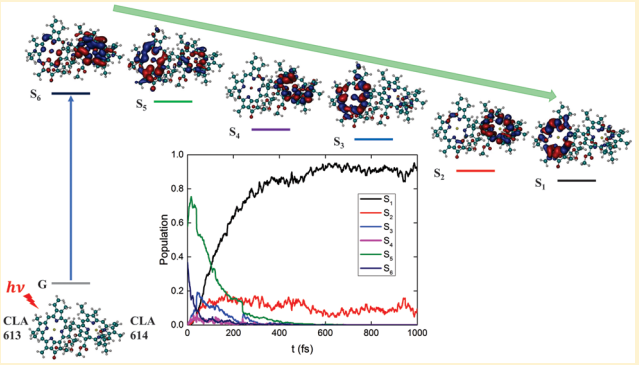

1. INTRODUCTION

Tasked to harvest solar photons and transform them into chemical energy with extremely high efficiency, photosynthesis is an essential biological process on the Earth. In natural photosynthetic systems, photons are absorbed by the light-harvesting complexes (LHCs) and excitation energy is then transferred to reaction centers where charge separation occurs.[1−4] Tremendous efforts have been devoted to studies of mechanisms underlying natural photosynthesis. A better understanding of the efficient energy transfer process also benefits the design of high fidelity artificial photosynthetic systems with superior robustness and efficiency.

Various photosynthetic organisms contain pigment−protein aggregates LHCs, such as the light-harvesting complex II (LHCII),[5] the Fenna−Matthews−Olson complex,[6−8] the light-harvesting complex 1[9] and the light-harvesting 2 (LH2) complex.[10,11] Wrapped by proteins, pigments such as chlorophylls (Chls), bacteriochlorophylls (Bchls), carotenoids and phycobilins are functional molecules for the photon absorption and subsequent excitation energy transfer processes.[1,4]

Acting as the main antenna in green plants, LHCII is the most abundant LHC in nature.[5,12] LHCII has a trimer structure (shown in Figure 1a) and each monomer contains various pigments, such as Chl*a* and Chl*b*. Solar energy can be absorbed by both Chl*a* and Chl*b*, and resulting excitation energy is transferred between the pigments. In addition to intermolecular energy transfer, the relaxation process from the high-lying energy excited states to the lowest excited state is another crucial step in excitation energy transfer in photosynthetic systems. Extensive efforts have been applied to study the internal conversion process in various photosynthetic pigments, such as Chl*a*,[13−17] Chl*b*,[13] Bchl*a*, and mutants of Bchl*a*.[18−20] However, only the internal conversion in an individual pigment is revealed in these investigations.[13−20] A pigment dimer is an ideal model to study the intermolecular energy transfer and the internal conversion details simultaneously.

Upon photoexcitation, nonradiative relaxation occurs from high-lying energy excited states to the lowest excited state of

Received: March 2, 2017
Revised: May 1, 2017
Published: May 8, 2017

DOI: 10.1021/acs.jpcb.7b02021
J. Phys. Chem. B 2017, 121, 5331−5339

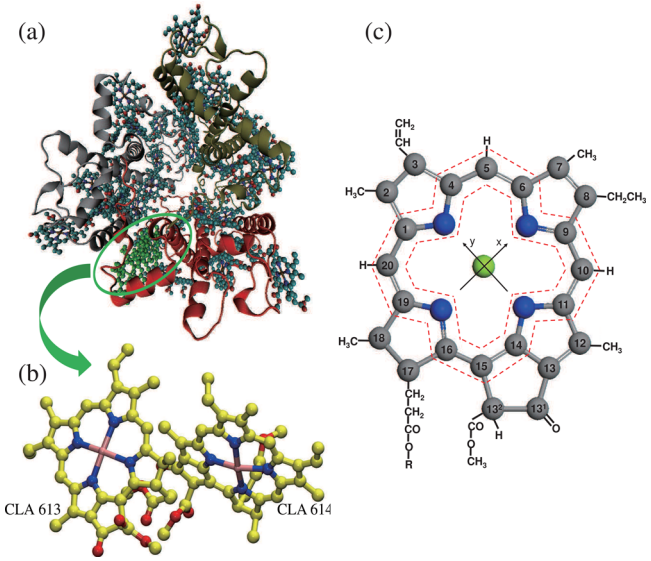

Figure 1. (a) Crystal structure of light-harvesting complex II (LHCII) from *Spinacia oleracea*[5] (PDB ID: 1RWT). (b) System simulated in this paper, chlorophyll*a* (Chl*a*) dimer in the LHCII complex. (c) Molecular structure of Chl*a*. Carbon (gray) atoms are labeled according to the IUPAC convention for porphyrins, with the standard x- and y- axes of Gouterman's four-orbital theory shown. The nitrogen and magnesium atoms are in blue and yellow, respectively. Chlorophyll phytyl tails (R) are replaced by a methyl group in the simulations. The total carbon macrocycle is defined as the carbon atoms comprising the porphyrin ring structure (carbon atoms 1−20 including atoms $C13^1$ and $C13^2$), whereas the "inner macrocycle" (atoms between two red dashed lines excluding the N atoms) consists of atoms C1, C4, C5, C6, C9, C10, C11, C14, C15, C16, C19, and C20, and the "outer macrocycle" is comprised of carbon atoms from the total carbon macrocycle minus those in the inner macrocycle.

pigments in photosynthetic pigment−protein complexes. As one of the key processes in the first step of photosynthesis, nonradiative relaxation in the single Chl*a* and Chl*b* molecules[13,14] has been studied with the nonadiabatic excited-state molecular dynamics (NA-ESMD).[21,22] The ratio of simulated relaxation constants in Chl*a* and Chl*b* monomers agreed well with that from ultrafast transient absorption spectroscopy. This approach has also been successfully applied to study ultrafast intramolecular exciton redistribution and energy relaxation after excitation in large-scale organic conjugated molecules.[22−26] In photosynthesis, intermolecular excitation energy relaxation is critical to energy transfer since many pigments are excited simultaneously and participate in global energy flux. It is therefore important to extend our investigations to the interpigment energy transfer, a fundamental process for the energy transfer in LHCs. In this work we apply the NA-ESMD method to investigate the energy transfer in a Chl*a* dimer (shown in Figure 1b) system.

The rest of the paper is organized as follows. The NA-ESMD methodology and computational details are described in section 2. Simulation results and discussions are presented in section 3 covering population dynamics, energy relaxation pathways, and inter- and intramonomer energy transfer in Chl*a* dimer. Conclusions are drawn in section 4.

2. THEORETICAL AND COMPUTATIONAL DETAILS

2.1. NA-ESMD Algorithm. The NA-ESMD algorithm[21,22] is suitable to investigate energy relaxation within multiple electronic excited states in large-scale organic molecules. In this algorithm, classical molecular dynamics (MD) is combined with the quantum transitions approach[27,28] in which excited-state energies,[29−31] gradients,[32,33] and nonadiabatic coupling terms[21,34−36] are computed with "on the fly" analytical calculations. This is achieved by applying the collective electron oscillator method[37−40] with the AM1 semiempirical Hamiltonian[41,42] at the configuration interaction singles (CIS) level.[43,44] Extensive previous studies have already adopted AM1 and similar semiempirical models to investigate excited state properties of porphyrin-based molecules.[23,42,45−54] The excited states calculated with the AM1/CIS method reproduce the measured energy gap between the Soret (B) band and the Q_y band, and has been successfully applied to calculate the excited states of Chl*a* and Chl*b* monomers.[13,14] A detailed discussion on parameter testings, algorithm implementation, advantages, and various applications of NA-ESMD can be found in the recent literature.[21,22,55]

2.2. Simulation Details. The crystal structure of the LHCII complex in *Spinacia oleracea*[5] (PDB ID: 1RWT) is adopted for our simulation. Two Chl*a* molecules (residues 613 and 614 in chain B of 1RWT) are selected in this work to simulate excited-state dynamics in the Chl*a* dimer system, and the orientation of the two pigments in the dimer is shown in Figure 1b.

First, we perform ground state MD simulation for the Chl*a* dimer from the initial structure for 520 ps at 300 K with a time step of 0.5 fs and four nitrogen atoms of Chl*a* molecules are fixed during the simulation to stabilize the relative molecular configurations in the absence of protein environment. The constant-temperature Langevin equation is adopted to describe the evolution of the nuclear degrees of freedom with a friction coefficient of 2.0 ps^{-1}. 500 snapshots from the last 500 ps simulation are extracted with a space of 1 ps, and every snapshot is then used to initialize another set of ground state MD simulation for 200 fs after releasing the constraints on the nitrogen atoms. The final configurations are used to compute absorption spectra and to perform the NA-ESMD of the Chl*a* dimer.

The absorption spectra are calculated for 500 configurations with 20 excited states considered. Shown in Figure 2 are the entire absorption spectra and contributions from all the excited states to the spectra. The first absorption band of Chl*a* dimer is around 1.69 eV which is red-shifted with respect to the first excited state (Q_y) of Chl*a* monomer (1.88 eV) due to interchromophore coupling. The second peak is at about 2.53 eV, and the third, at 2.91 eV close to the Soret band of the Chl*a* monomer. As it has been pointed out previously,[13] although the absolute excitation energies produced by semiempirical methods deviate from measurements, energy gaps between excited states agree with experimental findings. This agreement allows simulations to predict the overall time scales of nonradiative relaxation from the high-energy excited states in the B band to the lowest excited state Q_y in the Chl*a* monomer, in agreement with transient absorption pump−probe measurements.[13]

A Gaussian-shaped laser pulse is chosen to simulate photoexcitation on the configurations obtained from the ground state MD. Excited state α is initially populated according to a Franck−Condon window defined by $g_\alpha(\boldsymbol{r}; \boldsymbol{R}) = (f_\alpha/\Omega_\alpha^2) \exp[-T^2(E_{laser} - \Omega_\alpha)^2]$ where f_α is the normalized oscillator strength of state α with a frequency of Ω_α, $\boldsymbol{r}(\boldsymbol{R})$ is the electronic (nuclear) coordinate, and E_{laser} is the laser energy. In

DOI: 10.1021/acs.jpcb.7b02021
J. Phys. Chem. B 2017, 121, 5331−5339

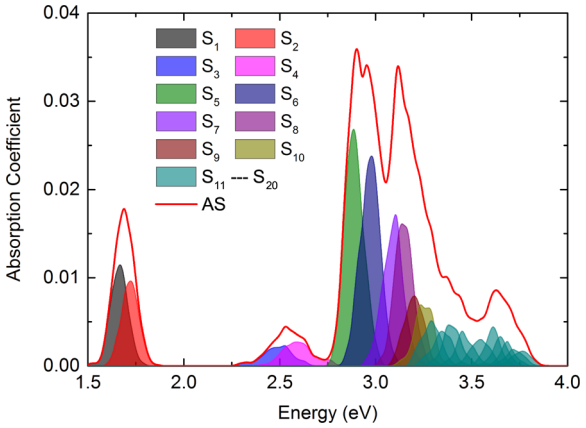

Figure 2. Absorption spectra of Chl*a* dimer. The red solid line is the integral absorption spectra obtained from the sampling results containing 500 molecular configurations. The colored profiles are the contributions of the first 20 excited states considered in the calculations to the final absorption spectra. The contributions of S_{11}−S_{20} are represented with gray profiles.

this study, the Gaussian-shaped laser pulse is centered at 2.93 eV (423 nm) with a standard deviation of 42.5 fs corresponding to a full width at half-maximum (fwhm) of 100 fs. A total of 500 independent excited state trajectories are calculated for 1 ps at 300 K, with a classical time-step of Δt = 0.1 fs and N_q = 4 quantum time steps per classical step to simultaneously propagate the coefficients of the electronic states. During the excited state dynamics, the 10 lowest excited states are taken into account for each trajectory.

2.3. Electronic Transition Density Analysis. To study exciton delocalization over the Chl*a* dimer, the electronic transition density (TD) is calculated as

$$(\rho^{g\alpha})_{nm} \equiv \langle \phi_\alpha(\mathbf{r};\mathbf{R}(t))|c_m^\dagger c_n|\phi_g(\mathbf{r};\mathbf{R}(t))\rangle \quad (1)$$

where $\phi_g(\boldsymbol{r};\boldsymbol{R}(t))$ ($\phi_\alpha(\boldsymbol{r};\boldsymbol{R}(t))$) is the wave function of the AM1/CIS adiabatic ground (excited) state, $c_m^\dagger$ (c_n) are the creation (annihilation) operators, and indices n and m refer to the atomic orbital basis functions. The diagonal elements $(\rho^{g\alpha})_{nn}$ represent the net change of the electronic density resulting from excitation from the ground state g to an electronic excited state α.[56] The normalization condition $\sum_n (\rho^{g\alpha})_{nn}^2 = 1$ is valid within the CIS approximation.[31] The fraction of the TD localized on different Chl*a* monomers, or arbitrary groups of atoms in the pigment can be obtained by summing up the atomic contributions belonging to each of them as

$$(\rho^{g\alpha})_X^2 = \sum_{n_A} (\rho^{g\alpha})_{n_A,n_A}^2 + \frac{1}{2}\sum_{n_B} (\rho^{g\alpha})_{n_B,n_B}^2 \quad (2)$$

where A is the index of atoms localized in the X-group, and the index B labels the atoms located at the interface of group X and another group.

3. RESULTS AND DISCUSSIONS

3.1. Population Dynamics. To investigate internal conversion dynamics in the Chl*a* dimer, we compute the average classical populations of the electronic states from an ensemble of 500 trajectories. The average populations for the first six excited states are shown in Figure 3. Here we can clearly see that nearly 90% of the excitation relaxes to the lowest excited states within 600 fs.

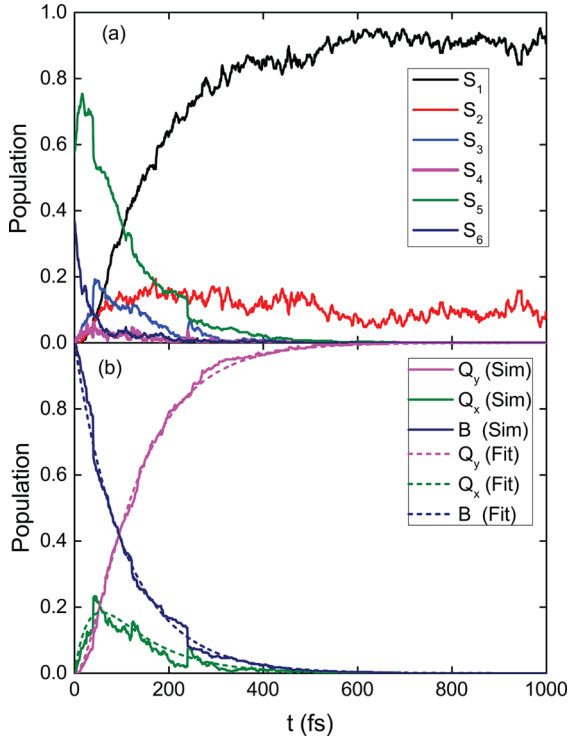

Figure 3. Calculated time evolution of classical population for (a) the lowest six electronic states and (b) three bands of Chl*a* dimer system. The results are averaged over 500 trajectories. Dashed lines in part b are the fitting curves of the band populations with the fitting parameters in Table 1.

According to the simulated absorption spectra of the Chl*a* dimer, we categorize the first 10 excited states in our simulations into three bands, i.e., Q_y, Q_x, and B bands. The S_1 and S_2 states yield the Q_y band while the S_3 and S_4 states contribute to the Q_x band. The B band is composed of excited states S_5−S_{10}. The average populations for these three bands are computed by summing the average populations of corresponding electronic states which belong to the bands.

To quantify the internal conversion rates in the Chl*a* dimer, we adopt a first-order monodirectional transfer model from B to Q_x and from Q_x to Q_y with rate constants k_1 and k_2, respectively. This yields the sequential transfer pathway $B \xrightarrow{k_1} Q_x \xrightarrow{k_2} Q_y$, to fit the average populations of these three bands.

The population of each band can then be given as

$$B(t) = B_0 e^{-k_1 t} \quad (3)$$

$$X(t) = \frac{k_1 B_0}{k_2 - k_1}(e^{-k_1 t} - e^{-k_2 t}) + X_0 e^{-k_2 t} \quad (4)$$

$$Y(t) = B_0 + X_0 + Y_0 - B(t) - X(t) \quad (5)$$

where B_0, X_0, and Y_0 represent the initial (t = 0) populations of the B, Q_x, and Q_y bands, respectively. The fitting is conducted through a least-squares regression analysis. The rate constants and the corresponding time constants ($\tau_1 = k_1^{-1}$, $\tau_2 = k_2^{-1}$) are presented in Table 1 in comparison to the respective

DOI: 10.1021/acs.jpcb.7b02021
J. Phys. Chem. B 2017, 121, 5331−5339

Table 1. Comparison of Internal Conversion Rates Obtained from a First-Order Irreversible Population Model for B → Q_x, Q_x → Q_y, and B → Q_y Pathways for Chl*a* Dimer and Monomer[13] Systems[a]

	B → Q_x		Q_x → Q_y		B → Q_y
system	k_1 (fs^{-1})	τ_1 (fs)	k_2 (fs^{-1})	τ_2 (fs)	τ_{tot} (fs)
monomer	0.0101	99.2 ± 1.1	0.007 81	128 ± 2	227 ± 3
dimer	0.009 24	108.2 ± 1.1	0.029 52	33.9 ± 0.7	142 ± 2

[a]Populations of specific excited states are averaged from 500 trajectories for Chl*a* dimer and 500 trajectories for Chl*a* monomer[13] in the NA-ESMD simulations.

parameters obtained for the Chl*a* monomer.[13] Shown in Figure 3b are the simulated population on the bands and the fitting results using modeled rate constants. The coefficients of determination (R^2) for the population curve fittings are 0.9958, 0.9192, and 0.9985 for B(t), $X(t)$, and $Y(t)$, respectively.

As shown in Table 1, the B → Q_x relaxation is marginally slower in the Chl*a* dimer than that in the Chl*a* monomer. In stark contrast, the dimer system has much faster Q_x → Q_y transfer rate compared to the Chl*a* monomer. Consequently, the overall relaxation from B to Q_y in the Chl*a* dimer (142 fs) is faster than that in the Chl*a* monomer (227 fs). For the Chl*a* dimer, each of the three energy bands is mainly composed of two electronic states as shown in Figure 2. As a result of the intermolecular electronic coupling and the configurational differences between the two monomers, there is a level splitting between the two electronic states (the so-called Davydov's pair) comprising the energy band of the Chl*a* dimer. The level splitting reduces the effective energy gaps between the absorption peaks of the Chl*a* dimer and enhances the relaxation efficiency between these energy bands.

Once the molecular system reaches the lowest Q_y band, there is a final relaxation step within the band. The population transfer from S_2 to S_1 exhibits contributions from two distinguished energy transfer regimes. As shown in Figure 3a, more than 95% of population transfer to the Q_y band occurs within 400 fs. In this time interval, the population of S_1 increases quickly as the electronic energy flows into the Q_y band. From 400 fs on, the energy of S_2 is transferred to S_1 slowly and leads to a gradual increase of the population on S_1. In order to reveal the fast and slow transfer components from S_2 to S_1, we fit the population of S_1 using the above model with the transfer rate from S_2 to S_1 being k_{S21}. It is assumed that in the transfer pathway B $\xrightarrow{k_1}$ Q_x $\xrightarrow{k_2}$ S_2 $\xrightarrow{k_{S21}}$ S_1, the energy of the Q_x band is first transferred to S_2 then from S_2 to S_1. This assumption is based on the fact that only a few hops to S_1 are observed from S_5 (6) and S_3 (29), which are negligible compared to an enormous number of hops from S_2 (3690) to S_1. Here, the population of S_2 can be fitted by the equation

$$S_2(t) = ae^{-k_1 t} + be^{-k_2 t} + ce^{-k_{S21} t} + S_{2_0}e^{-k_{S21} t} \quad (6)$$

with

$$a = -\frac{B_0 k_1 k_2}{(k_1 - k_2)(k_{S21} - k_1)}$$

$$b = \frac{B_0 k_1 k_2 + k_1 k_2 X_0 - k_2^2 X_0}{(k_1 - k_2)(k_{S21} - k_2)}$$

and

$$c = \frac{B_0 k_1 k_2 - k_2 k_{S21} X_0 + k_1 k_2 X_0}{(k_{S21} - k_1)(k_{S21} - k_2)}$$

Subsequently, the population of S_1 is

$$S_1(t) = B_0 + X_0 + S_2(0) + S_1(0) - B(t) - X(t) - S_2(t) \quad (7)$$

We fit the population of S_1 in these two time intervals with eq 7 as shown in Figure 4. By fitting the first 400 fs and

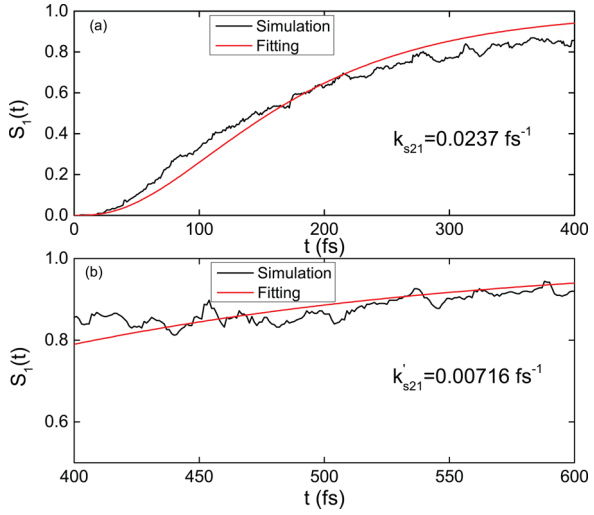

Figure 4. Population of S_1 averaged from 500 trajectories and fitting results with eq 7 for fast (a) and slow (b) regimes.

subsequent 400−600 fs time-intervals of relaxation dynamics, we obtain the fast k_{S21} = 0.0237 fs^{-1} ($\tau_{S21} = k_{S21}^{-1}$ = 42.19 fs) and slow k'_{S21} = 0.00716 fs^{-1} (τ'_{S21} = 139.66 fs) transfer rates, respectively.

3.2. Initial Exciton Localization. We analyze exciton localization of various electronic excited states at the moment of Franck−Condon photoexcitation from ground state configurations equilibrated at 300 K. For a certain configuration, a reference monomer is selected as the monomer which has a higher fraction of TD of S_1 [$(\rho^{01})^2_{monomer} > 0.5$] initially, and is denoted as HM of S_1. Then we obtain the TD distributions of the other states (S_2 − S_6) on the reference monomer by constructing histograms of the TD for all initial configurations. Roughly, half of the total configurations (i.e., 243 or 48.6% out of 500 configurations) have monomer CLA 613 as their HM of S_1.

The initial distribution of all the states on the HM of S_1 is shown in Figure 5. It is clearly seen that S_1 is strongly localized on its HM. The TD of all other electronic states are distributed near 0 and 1 which indicates persistent localization on a single monomer for all cases. As expected, for most configurations, S_1 and S_3 are initially localized on the same monomer while S_2 and S_4 are localized on the other monomer. High-lying energy states S_5 and S_6 seem to be ambiguously localized on any chromophore. Thus, in spite of significant electronic coupling

DOI: 10.1021/acs.jpcb.7b02021
J. Phys. Chem. B 2017, 121, 5331−5339

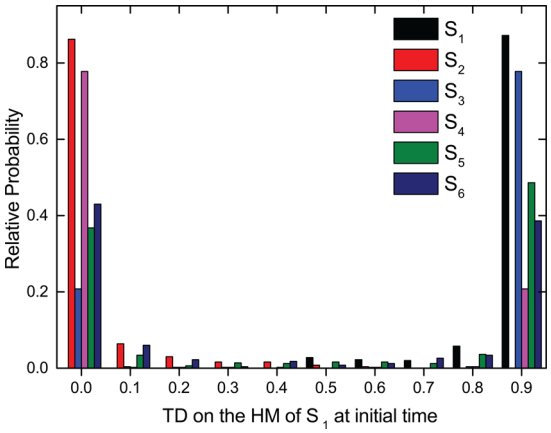

Figure 5. Distribution of the transition density for the electronic states on the higher monomer of S_1 at initial time (500 configurations).

between monomers, which splits the electronic states, thermal fluctuations at room temperature essentially localize the excited state wave function initially to a single Chl*a* in a dimer configuration.

3.3. Energy Relaxation Pathways. Subsequent to photoexcitation, the Chl*a* dimer experiences an efficient B band → Q_y band transition. According to the fewest switches surface hopping algorithm[27] implemented in our NA-ESMD simulations, electronic transitions are described as hops from one initial electronic state S_i to another S_f final state. The relative probabilities of effective $S_i \rightarrow S_f$ transitions during all the NA-ESMD simulations are summarized in Table 2. An effective $S_i \rightarrow S_f$ transition refers as $S_i \rightarrow S_f$ hops for which no back-hopping $S_f \rightarrow S_i$ occurs along the rest time of this NA-ESMD trajectory. The relative probabilities have been normalized for hops corresponding to the same S_i state.

Table 2. Fraction of Effective Transitions from S_i to S_f ($S_i > S_f$)

	S_i				
S_f	S_6	S_5	S_4	S_3	S_2
S_5	0.97	–	–	–	–
S_4	0.02	0.78	–	–	–
S_3	0.01	0.21	1.0	–	–
S_2	0	0	0	0.95	–
S_1	0	0.01	0	0.05	1.0

We can clearly see from the data in Table 2 that the relaxation mainly takes place along the sequential pathway $S_6 \rightarrow S_5 \rightarrow S_4 \rightarrow S_3 \rightarrow S_2 \rightarrow S_1$ in the Chl*a* dimer. Transitions from S_6 to S_5, S_4 and S_3 occur with relative probabilities of 0.97, 0.02 and 0.01, respectively. According to the ambiguous initial localization of this state (see Figure 5) these initial relaxation steps involve both intra- and inter- monomer energy transfer events. In the case of effective hops from S_5, the sequential pathway to S_4 takes up 78% of its energy transfer flux and, according to Figure 5, it involves mainly an intermonomer energy transfer. The intramonomer $S_5 \rightarrow S_3$ channel accounts for the remainder 21%. In contrast, effective hops from S_4 mostly develop only through the intermonomer channel to S_3. The intermonomer channel of $S_3 \rightarrow S_2$ occupies 95% of the relaxation from S_3 while the intramonomer channel holds a minor 5% contribution, followed by a final intermonomer $S_2 \rightarrow S_1$ relaxation.

3.4. Transient Electronic Transition Density Redistribution. Summarizing the above observations, B → Q_y internal conversion process after photoexcitation of the Chl*a* dimer takes place mainly through a sequential cascade mechanism involving multiple exciton exchanges between monomers. Notably, a localization pattern shown in Figure 5 is getting significantly perturbed by the dynamics, i.e., the wave function should not necessarily remain localized on a single Chl*a*, which is subject to analysis in this section. Namely, the time evolution of the photoinduced inter- and intra- monomer electronic transition can be tracked by TD redistribution in the Chl*a* dimer. Thus, complementary studies of the exciton spatial localization in the trajectory ensemble reveal a comprehensive picture on the interplay of concomitant inter- and intra-monomer relaxation processes.

3.4.1. Intermonomer Exciton Exchange. The Chl*a* dimer considered in this study is composed of CLA 613 and CLA 614 residues from the chain B of the crystal structure 1RWT of LHCII. The laser excitation leads to nearly equivalent probabilities for the two residues to become excited initially. In Figure 6a, we show the time evolution of the average fraction of TD on CLA 613 ($(\rho^{0\alpha})^2_{\mathrm{CLA\ 613}}$). Its value fluctuates around 0.6, indicating a slightly higher tendency of the exciton to get trapped on it.

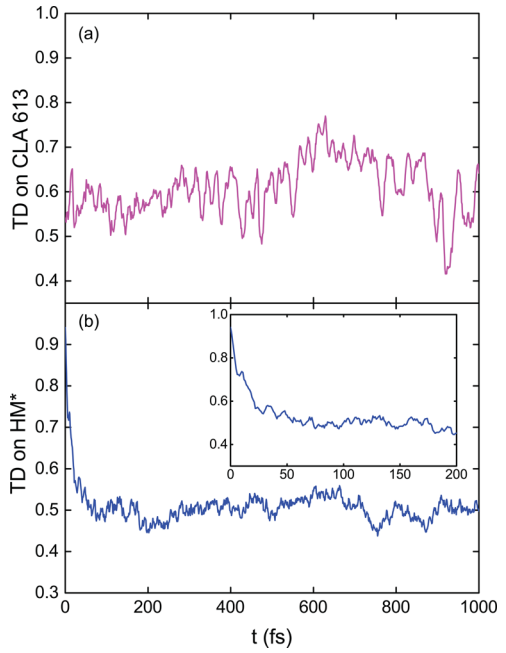

Figure 6. Fraction of electronic transition density localized on (a) the monomer CLA 613 and (b) the higher monomer (HM*) being averaged over all trajectories.

In order to further investigate signatures of exciton delocalization between the two monomers, we define the higher monomer (HM*) as the monomer with the higher fraction of TD in the current excited state at the initial time, $(\rho^{0\alpha})^2_{\mathrm{HM*}}(t = 0) > 0.5$. It is important to stress that, according with the given definition, HM* can be either CLA 613 or CLA 614 residues and it should be chosen individually for each NA-ESMD trajectory. Once the HM* has been selected at $t = 0$ for each trajectory, it remains the same throughout this NA-ESMD simulation. The time evolution of the average over all trajectories of $(\rho^{0\alpha})^2_{\mathrm{HM*}}$ is depicted in Figure 6b. HM*

DOI: 10.1021/acs.jpcb.7b02021
J. Phys. Chem. B 2017, 121, 5331−5339

corresponds to CLA 613 for 53.6% of trajectories. As a result of an ultrafast effective intermonomer exciton exchange, the value of $(\rho^{0\alpha})^2_{HM*}$ experiences an ultrafast decrease during the first ~100 fs. Its final value of ~0.5 may follow from two possible scenarios. In one scenario, a true delocalized electronic state can be equally shared by two monomers, and in the second, it can result from localized states that hop between monomers. In order to distinguish between these scenarios, we further analyze the participation number which is defined as

$$P = [((\rho^{0\alpha})^2_{\mathrm{CLA\ 613}})^2 + ((\rho^{0\alpha})^2_{\mathrm{CLA\ 614}})^2]^{-1} \quad (8)$$

where $(\rho^{0\alpha})^2_{\mathrm{CLA\ 613}}$ ($(\rho^{0\alpha})^2_{\mathrm{CLA\ 614}}$) is the fraction of TD localized on monomer CLA 613 (614). The value of P varies in the interval between 1 and 2 as each monomer is treated as a unit. If $P \approx 1$, it means that the TD is almost completely localized on a single Chl*a* monomer, while $P \approx 2$ means that the TD is delocalized over the two Chl*a* monomers. The time evolution of the average value of P during the NA-ESMD simulation is shown in Figure 7. As can be seen, the initial excitation

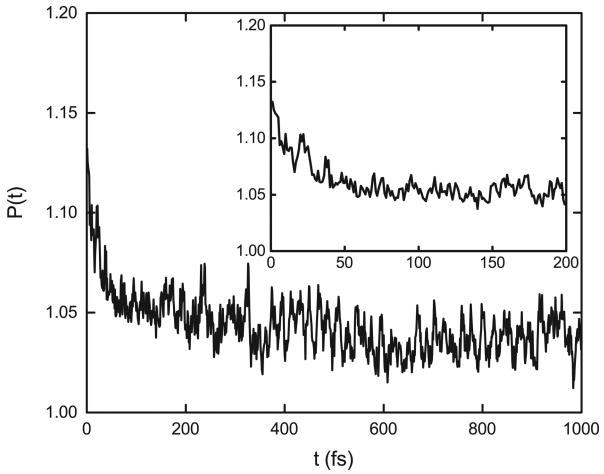

Figure 7. Time evolution of the participation number of Chl*a* dimer taken as an average over all trajectories.

effectively generates a weakly delocalized state between the two monomers. Thereafter, the excited state dynamics leads to an almost complete localization of the TD to one monomer within ~100 fs.

The intermonomer exciton exchanges throughout the NA-ESMD simulations can be further analyzed by events with significant changes of $(\rho^{0\alpha})^2_{\mathrm{monomer}}$. Figure 8a displays the time dependence of the relative probability of exciton-exchange events between monomers. An event of significant TD exchange between monomers is considered when $\Delta(\rho^{0\alpha})^2_{\mathrm{monomer}} > 0.5$. Despite larger probabilites at earlier times, the intermonomer energy exchange persists thoughout the simulations, highlighting the main role of the intermonomer pathway during the internal conversion process of the Chl*a* dimer. Therefore, the average number of exciton hops between monomers per NA-ESMD simulation is relatively high (~38) (see Figure 8b).

Energy relaxation through localized states on the individual chromophores can be explained by analyzing coupling between states belonging to each band, that is, S_1 and S_2 for Q_y, S_3 and S_4 for Q_x, and S_5 to S_{10} for B band. The coupling is computed as half of the energy splitting between two excited states of the Chl*a* dimer, and both the Förster and the Dexter contributions

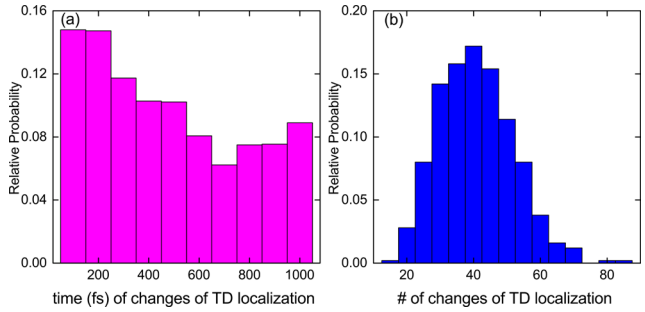

Figure 8. (a) Relative probability of exciton exchange between monomers as a function of time. (b) Histogram of the number of TD localization changes between the monomers during the NA-ESMD simulations.

to the coupling can be included.[57,58] This method has been successfully applied to estimate the electronic coupling between the pigments in LH2 (e.g., ref 58). Our calculations on all 500 initial configurations, obtained from the equilibrated ground state MD simulation, are shown in Table 3. Considering

Table 3. Average Excitation Energy and Full Width at Half Maximum (Fwhm) Extracted from the Gaussian Fitting of the Excitation Energy Distribution from 500 Configurations

band	excited state	average excitation energy (eV)	fwhm (eV)
Q_y	1	1.669	0.104
	2	1.725	0.101
Q_x	3	2.478	0.177
	4	2.577	0.173
B	5	2.889	0.116
	6	2.978	0.120
	7	3.094	0.136
	8	3.156	0.111
	9	3.207	0.114
	10	3.252	0.117

coupling as half of the energy splitting between states, we obtained average values of 224 and 398 cm^{-1} for Q_y and Q_x bands, respectively. On the basis of the four-orbital model for porphyrins,[59,60] the B band of chlorophylls are composed of two bands, namely, the B_x and B_y bands.[61,62] For the Chl*a* dimer studied in this work, we assign S_5 and S_6 to the B_x band, and S_7 and S_8 to the B_y band, respectively. Then we obtain a coupling strength of 360 cm^{-1}(250 cm^{-1}) between the states in B_x (B_y) band. The Q_y–Q_y and B_x–B_x coupling strengths computed here agree well with previous results obtained for the LH2 pigments.[58] Compare to the Q_y–Q_y coupling estimated by the dipole–dipole interaction approximation[63] and the Poisson-TrEsp method,[64] we obtain relatively stronger Q_y–Q_y coupling in this work as a result of excluding protein environments. As can be seen, the strength of the thermal fluctuations (fwhm of the excitation energy distribution) do exceed the coupling which leads to localized states on individual chromophores. Excited state dynamics then separates the states even further due to vibrational relaxation. However, in the phase space domains where electronic states are strongly coupled, states become nearly degenerate promoting delocalization as a Frenkel exciton and facilitating thus efficient interchromophore energy transfer.

3.4.2. Intramonomer Exciton Redistribution. During the internal conversion process of the Chl*a* dimer, each monomer

DOI: 10.1021/acs.jpcb.7b02021
J. Phys. Chem. B 2017, 121, 5331−5339

experiences an intramolecular wave function redistribution. We monitor the fractions of TD localized on specific atoms, functional groups, and regions of each Chl*a* monomer. The structure of the Chl*a* molecule is depicted in Figure 1c. Following our previous work on the Chl*a* monomer,[14] the porphyrin ring of the molecule is fragmented into following groups, i.e., atom Mg, atoms N, and the inner and the outer macrocycle. The total carbon macrocycle contains the carbon atoms comprising the porphyrin ring structure (carbon atoms 1−20 including atoms $C13^1$ and $C13^2$). The "inner macrocycle" (atoms between two red dashed lines excluding the N atoms in Figure 1c) is comprised of atoms C1, C4, C5, C6, C9, C10, C11, C14, C15, C16, C19, and C20. The "outer macrocycle" consists of carbon atoms in the total carbon macrocycle excluding those in the inner macrocycle.

For each trajectory, we denote the HM* (LM*) as the monomer which has higher (lower) fraction of TD in the current excited state initially. We depict the time evolution of the averaged TD localized on each partition of the porphyrin ring of either HM* and LM* in Figure 9a−d. Within ∼100 fs,

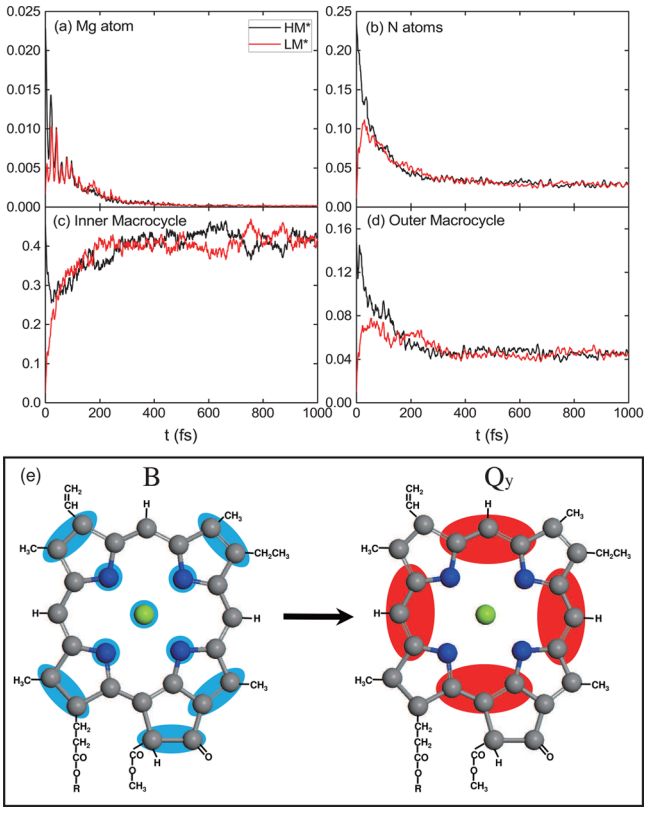

Figure 9. Time evolution of the averaged TD localized on the (a) Mg atom, (b) N atoms, (c) inner macrocycle, and (d) outer macrocycle for higher monomer (HM*) and lower monomer (LM*). (e) Schematic representation for the predominant transition density redistribution on a chlorophyll *a* monomer during the conversion from B to Q_y. Background areas with blue and red colors represent the transition density for the B and Q_y bands, respectively.

the fractions of TD on specific atoms (Mg and N atoms), and regions (inner and outer carbon macrocycles) of LM* approach those of HM*. The overall TD redistribution on a monomer during the conversion from B to Q_y is analyzed and depicted in Figure 9e. The intramolecular exciton redistribution within each monomer of the Chl*a* dimer reproduces results previously found in individual Chl*a* molecules.[14] That is, the overall B → Q_y energy relaxation implies the transfer of localized TD from the N atoms and the outer carbon macrocycle to the inner carbon macrocycle, and the central Mg atoms play minor roles in the exciton relocalization.

4. CONCLUSIONS

Electronic dynamics simulations beyond the Born−Oppenheimer approximation have been carried out to investigate photoinduced intra- and inter- chromophore energy transfer in a Chl*a* dimer at the interface of two units of LHCII trimer from *Spinacia oleracea*.[5] It is found that the overall B →Q_y internal conversion in a Chl*a* dimer to be faster than that in an isolated Chl*a* monomer. Indeed, dimerization induced energy level splittings in a molecular pair effectively reduce the energy gaps between the excited states and ultimately lead to a faster relaxation rate compared to a single chromophore. Our analysis of electronic transition density dynamics signified by its redistribution in the Chl*a* dimer reveals competition between concomitant inter- and intra- monomer relaxation processes. The initial laser excitation generates a weakly delocalized state. The strength of thermal fluctuations generally exceeds electronic coupling between states, leading to quasi-localized states on the individual chromophores. The excited state dynamics triggers vibrational relaxation and a complete state localization. However, in the phase space domains where electronic states are strongly coupled, states become nearly degenerate promoting exciton delocalization and facilitating efficient interchromophore energy transfer. The internal conversion process proceeds mainly through a sequential-cascade pathway $S_6 \rightarrow \cdots \rightarrow S_1$ involving multiple exciton exchanges between monomers. Once the molecular system reaches the lowest Q_y band, the final $S_2 \rightarrow S_1$ relaxation step takes significantly longer time. The intermolecular energy exchange still persists throughout the entire 1 ps dynamics, highlighting the main role of the intermonomer pathway during the internal conversion process in the Chl*a* dimer. As nonradiative relaxation develops, energy redistribution on two Chl*a* molecules yields nearly equal distribution of the exciton among the monomers due to incoherent exciton hopping between localized excited states. Despite the intermonomer exciton exchanges, the intramolecular exciton redistribution within each monomer of the Chl*a* dimer reproduces results previously found in individual Chl*a* molecules.[14]

AUTHOR INFORMATION

Corresponding Authors

*(S.F.-A.) E-mail: sfalberti@gmail.com.

*(Y.Z.) E-mail: yzhao@ntu.edu.sg. Telephone: +(65) 65137990.

ORCID

Sergei Tretiak: 0000-0001-5547-3647

Yang Zhao: 0000-0002-7916-8687

Notes

The authors declare no competing financial interest.

ACKNOWLEDGMENTS

F.Z. would like to thank Prathamesh Shenai for helpful discussion. The authors acknowledge support from the Singapore National Research Foundation through the Competitive Research Programme (CRP) under Project No. NRF-CRP5-2009-04. Support from the Singapore Ministry of

DOI: 10.1021/acs.jpcb.7b02021
J. Phys. Chem. B 2017, 121, 5331−5339

Education Academic Research Fund Tier 1 (Grant No. RG106/15) is also gratefully acknowledged. S.T. acknowledges support from the Center for Integrated Nanotechnology (CINT), a U.S. Department of Energy, Office of Basic Energy Sciences user facility (under Contract DE-AC52-06NA25396). S.F.-A is supported in part by CONICET, UNQ, and ANPCyT (PICT-2014-2662).

REFERENCES

(1) Blankenship, R. E. *Molecular Mechanisms of Photosynthesis*; Blackwell Publishing: Williston, VT, 2002.
(2) Croce, R.; van Amerongen, H. Natural Strategies for Photosynthetic Light Harvesting. *Nat. Chem. Biol.* **2014**, *10*, 492−501.
(3) Scholes, G. D.; Fleming, G. R.; Olaya-Castro, A.; van Grondelle, R. Lessons from Nature about Solar Light Harvesting. *Nat. Chem.* **2011**, *3*, 763−774.
(4) Rabinowitch, E.; Govindjee *Photosynthesis*; Wiley: New York, 1969.
(5) Liu, Z.; Yan, H.; Wang, K.; Kuang, T.; Zhang, J.; Gui, L.; An, X.; Chang, W. Crystal Structure of Spinach Major Lightharvesting Complex at 2.72 Å Resolution. *Nature* **2004**, *428*, 287−292.
(6) Fenna, R. E.; Matthews, B. W. Chlorophyll Arrangement in a Bacteriochlorophyll Protein from Chlorobium limicola. *Nature* **1975**, *258*, 573−577.
(7) Li, Y. F.; Zhou, W. L.; Blankenship, R. E.; Allen, J. P. Crystal Structure of the Bacteriochlorophyll a Protein from Chlorobium tepidum. *J. Mol. Biol.* **1997**, *271*, 456−471.
(8) Camara-Artigas, A.; Blankenship, R. E.; Allen, J. P. The Structure of the FMO Protein from Chlorobium tepidum at 2.2 Angstrom Resolution. *Photosynth. Res.* **2003**, *75*, 49−55.
(9) Karrasch, S.; Bullough, P. A.; Ghosh, R. The 8.5 Å Projection Map of the Lightharvesting Complex I from Rhodospirillum rubrum Reveals a Ring Composed of 16 Subunits. *EMBO J.* **1995**, *14*, 631−638.
(10) McDermott, G.; Prince, S. M.; Freer, A. A.; Hawthornthwaitelawless, A. M.; Papiz, M. Z.; Cogdell, R. J.; Isaacs, N. W. Crystal Structure of an Integral Membrane Light-harvesting Complex from Photosynthetic Bacteria. *Nature* **1995**, *374*, 517−521.
(11) Koepke, J.; Hu, X.; Muenke, C.; Schulten, K.; Michel, H. The Crystal Structure of the Light-harvesting Complex II (B800−850) from Rhodospirillum molischianum. *Structure* **1996**, *4*, 581−597.
(12) Enriquez, M. M.; Akhtar, P.; Zhang, C.; Garab, G.; Lambrev, P. H.; Tan, H.-S. Energy Transfer Dynamics in Trimers and Aggregates of Light-harvesting Complex II Probed by 2D Electronic Spectroscopy. *J. Chem. Phys.* **2015**, *142*, 212432.
(13) Bricker, W. P.; Shenai, P. M.; Ghosh, A.; Liu, Z.; Enriquez, M. G. M.; Lambrev, P. H.; Tan, H. S.; Lo, C. S.; Tretiak, S.; Fernandez Alberti, S.; Zhao, Y. Non-radiative Relaxation of Photoexcited Chlorophylls: Theoretical and Experimental Study. *Sci. Rep.* **2015**, *5*, 13625.
(14) Shenai, P. M.; Fernandez-Alberti, S.; Bricker, W. P.; Tretiak, S.; Zhao, Y. Internal Conversion and Vibrational Energy Redistribution in Chlorophyll A. *J. Phys. Chem. B* **2016**, *120*, 49−58.
(15) Shi, Y.; Liu, J. Y.; Han, K. L. Investigation of the Internal Conversion Time of the Chlorophyll a from S3, S2 to S1. *Chem. Phys. Lett.* **2005**, *410*, 260−263.
(16) Dong, L. Q.; Niu, K.; Cong, S. L. Theoretical Study of Vibrational Relaxation and Internal Conversion Dynamics of Chlorophyll-a in Ethyl Acetate Solvent in Femtosecond Laser Fields. *Chem. Phys. Lett.* **2006**, *432*, 286−290.
(17) Dong, L. Q.; Niu, K.; Cong, S. L. Theoretical Analysis of Internal Conversion Pathways and Vibrational Relaxation Process of Chlorophyll-a in Ethyl Ether Solvent. *Chem. Phys. Lett.* **2007**, *440*, 150−154.
(18) Kosumi, D.; Nakagawa, N.; Sakai, S.; Nagaoka, Y.; Maruta, S.; Sugisaki, M.; Dewa, T.; Nango, M.; Hashimoto, H. Ultrafast Intramolecular Relaxation Dynamics of Mg- and Zn-bacteriochlorophyll a. *J. Chem. Phys.* **2013**, *139*, 034311.
(19) Musewald, C.; Hartwich, G.; Lossau, H.; Gilch, P.; Pöllinger-Dammer, F.; Scheer, H.; Michel-Beyerle, M. E. Ultrafast Photophysics and Photochemistry of [Ni]-bacteriochlorophyll a. *J. Phys. Chem. B* **1999**, *103*, 7055−7060.
(20) Kosumi, D.; Maruta, S.; Fujii, R.; Kanemoto, K.; Sugisaki, M.; Hashimoto, H. Ultrafast Excited State Dynamics of Monomeric Bacteriochlorophyll a. *Phys. Status Solidi C* **2011**, *8*, 92−95.
(21) Nelson, T.; Fernandez-Alberti, S.; Chernyak, V.; Roitberg, A. E.; Tretiak, S. Nonadiabatic Excited-State Molecular Dynamics Modeling of Photoinduced Dynamics in Conjugated Molecules. *J. Phys. Chem. B* **2011**, *115*, 5402−5414.
(22) Nelson, T.; Fernandez-Alberti, S.; Roitberg, A.; Tretiak, S. Nonadiabatic Excited-State Molecular Dynamics: Modeling Photophysics in Organic Conjugated Materials. *Acc. Chem. Res.* **2014**, *47*, 1155−1164.
(23) Alfonso Hernandez, L.; Nelson, T.; Tretiak, S.; Fernandez Alberti, S. Photoexcited Energy Transfer in a Weakly Coupled Dimer. *J. Phys. Chem. B* **2015**, *119*, 7242−7252.
(24) Oldani, N.; Tretiak, S.; Bazan, G.; Fernandez-Alberti, S. Modeling of Internal Conversion in Photoexcited Conjugated Molecular Donor Used in Organic Photovoltaics. *Energy Environ. Sci.* **2014**, *7*, 1175−1184.
(25) Adamska, L.; Nayyar, I.; Chen, H.; Swan, A. K.; Oldani, N.; Fernandez-Alberti, S.; Golder, M. R.; Jasti, R.; Doorn, S. K.; Tretiak, S. Self-Trapping of Excitons, Violation of Condon Approximation, and Efficient Fluorescence in Conjugated Cycloparaphenylenes. *Nano Lett.* **2014**, *14*, 6539−6546.
(26) Ondarse-Alvarez, D.; Oldani, N.; Tretiak, S.; Fernandez-Alberti, S. Computational Study of Photoexcited Dynamics in Bichromophoric Cross-shaped Oligofluorene. *J. Phys. Chem. A* **2014**, *118*, 10742−10753.
(27) Tully, J. C. Molecular-Dynamics with Electronic-Transitions. *J. Chem. Phys.* **1990**, *93*, 1061−1071.
(28) Hammes-Schiffer, S.; Tully, J. C. Proton-Transfer in Solution-Molecular-Dynamics with Quantum Transitions. *J. Chem. Phys.* **1994**, *101*, 4657−4667.
(29) Tretiak, S.; Mukamel, S. Density Matrix Analysis and Simulation of Electronic Excitations in Conjugated and Aggregated Molecules. *Chem. Rev.* **2002**, *102*, 3171−3212.
(30) Chernyak, V.; Schulz, M. F.; Mukamel, S.; Tretiak, S.; Tsiper, E. V. Krylov-Space Algorithms for Time-Dependent Hartree-Fock and Density Functional Computations. *J. Chem. Phys.* **2000**, *113*, 36−43.
(31) Tretiak, S.; Isborn, C. M.; Niklasson, A. M. N.; Challacombe, M. Representation Independent Algorithms for Molecular Response Calculations in Time-Dependent Self-Consistent Field Theories. *J. Chem. Phys.* **2009**, *130*, 054111.
(32) Furche, F.; Ahlrichs, R. Adiabatic Time-Dependent Density Functional Methods for Excited State Properties. *J. Chem. Phys.* **2002**, *117*, 7433−7447.
(33) Tretiak, S.; Chernyak, V. Resonant Nonlinear Polarizabilities in the Time-Dependent Density Functional Theory. *J. Chem. Phys.* **2003**, *119*, 8809−8823.
(34) Tommasini, M.; Chernyak, V.; Mukamel, S. Electronic Density-Matrix Algorithm for Nonadiabatic Couplings in Molecular Dynamics Simulations. *Int. J. Quantum Chem.* **2001**, *85*, 225−238.
(35) Chernyak, V.; Mukamel, S. Density-Matrix Representation of Nonadiabatic Couplings in Time-Dependent Density Functional (TDDFT) Theories. *J. Chem. Phys.* **2000**, *112*, 3572−3579.
(36) Send, R.; Furche, F. First-Order Nonadiabatic Couplings from Time-Dependent Hybrid Density Functional Response Theory: Consistent Formalism, Implementation, and Performance. *J. Chem. Phys.* **2010**, *132*, 044107.
(37) Mukamel, S. Photochemistry-Trees to Trap Photons. *Nature* **1997**, *388*, 425−427.
(38) Mukamel, S.; Tretiak, S.; Wagersreiter, T.; Chernyak, V. Electronic Coherence and Collective Optical Excitations of Conjugated Molecules. *Science* **1997**, *277*, 781−787.

DOI: 10.1021/acs.jpcb.7b02021
J. Phys. Chem. B 2017, 121, 5331−5339

(39) Tretiak, S.; Chernyak, V.; Mukamel, S. Recursive Density-Matrix-Spectral-Moment Algorithm for Molecular Nonlinear Polarizabilities. *J. Chem. Phys.* **1996**, *105*, 8914−8928.
(40) Tretiak, S.; Zhang, W. M.; Chernyak, V.; Mukamel, S. Excitonic Couplings and Electronic Coherence in Bridged Naphthalene Dimers. *Proc. Natl. Acad. Sci. U. S. A.* **1999**, *96*, 13003−13008.
(41) Dewar, M. J. S.; Zoebisch, E. G.; Healy, E. F.; Stewart, J. J. P. AM1: A New General Purpose Quantum Mechanical Model. *J. Am. Chem. Soc.* **1985**, *107*, 3902−3909.
(42) Stewart, J. J. P. Optimization of Parameters for Semiempirical Methods IV: Extension of MNDO, AM1, and PM3 to More Main Group Elements. *J. Mol. Model.* **2004**, *10*, 155−164.
(43) Shavitt, I. *Modern Theoretical Chemistry*; Plenum Press: New York, 1976.
(44) Szalay, P. G.; Müller, T.; Gidofalvi, G.; Lischka, H.; Shepard, R. Multiconfiguration Self-Consistent Field and Multireference Configuration Interaction Methods and Applications. *Chem. Rev.* **2012**, *112*, 108−181.
(45) Reynolds, C. H. An AM1 Theoretical Study of the Structure and Electronic Properties of Porphyrin. *J. Org. Chem.* **1988**, *53*, 6061−6064.
(46) Zandler, M. E.; D'Souza, F. Electronic and Structural Properties of the Metalloporphyrin Structural Isomers: Semiempirical AM1 and PM3 Calculations. *J. Mol. Struct.: THEOCHEM* **1997**, *401*, 301−314.
(47) Katagi, T. Semi-Empirical AM1 and PM3 Calculations of Five- and Six-Coordinate Oxo Iron (iv) Porphyrin Complexes. *J. Mol. Struct.: THEOCHEM* **2005**, *728*, 49−56.
(48) Stewart, J. J. P. Optimization of Parameters for Semiempirical Methods I. Method. *J. Comput. Chem.* **1989**, *10*, 209−220.
(49) Stewart, J. J. P. Optimization of Parameters for Semiempirical Methods II. Applications. *J. Comput. Chem.* **1989**, *10*, 221−264.
(50) Stewart, J. J. P. Optimization of Parameters for Semiempirical Methods III. Extension of PM3 to Be, Mg, Zn, Ga, Ge, As, Se, Cd, In, Sn, Sb, Te, Hg, Tl, Pb, and Bi. *J. Comput. Chem.* **1991**, *12*, 320−341.
(51) Linnanto, J.; Korppi-Tommola, J. Spectroscopic Properties of Mg-chlorin, Mg-porphyrin and chlorophylls *a*, *b*, *c1*, *c2*, *c3* and *d* Studied by Semi-Empirical and *ab initio* MO/CI methods. *Phys. Chem. Chem. Phys.* **2000**, *2*, 4962−4970.
(52) Linnanto, J.; Korppi-Tommola, J. Spectroscopic Properties of Mg-chlorin, Mg-bacterochlorin and Bacteriochlorophylls *a*, *b*, *c*, *d*, *e*, *f*, *g*, and *h* Studied by Semiempirical and *ab initio* MO/CI Methods. *J. Phys. Chem. A* **2001**, *105*, 3855−3866.
(53) Linnanto, J.; Korppi-Tommola, J. Quantum Chemical Simulation of Excited States of Chlorophylls, Bacteriochlorophylls and Their Complexes. *Phys. Chem. Chem. Phys.* **2006**, *8*, 663−687.
(54) Nguyen, K. A.; Day, P. N.; Pachter, R.; Tretiak, S.; Chernyak, V.; Mukamel, S. Analysis of Absorption Spectra of Zinc Porphyrin, Zinc *meso*-Tetraphenylporphyrin, and Halogenated Derivatives. *J. Phys. Chem. A* **2002**, *106*, 10285−10293.
(55) Nelson, T.; Fernandez-Alberti, S.; Chernyak, V.; Roitberg, A. E.; Tretiak, S. Nonadiabatic Excited-State Molecular Dynamics: Numerical Tests of Convergence and Parameters. *J. Chem. Phys.* **2012**, *136*, 054108.
(56) Wu, C.; Malinin, S. V.; Tretiak, S.; Chernyak, V. Y. Multiscale Modeling of Electronic Excitations in Branched Conjugated Molecules Using an Exciton Scattering Approach. *Phys. Rev. Lett.* **2008**, *100*, 057405.
(57) Tretiak, S.; Middleton, C.; Chernyak, V.; Mukamel, S. Exciton Hamiltonian for the Bacteriochlorophyll System in the LH2 Antenna Complex of Purple Bacteria. *J. Phys. Chem. B* **2000**, *104*, 4519−4528.
(58) Tretiak, S.; Middleton, C.; Chernyak, V.; Mukamel, S. Bacteriochlorophyll and Carotenoid Excitonic Couplings in the LH2 System of Purple Bacteria. *J. Phys. Chem. B* **2000**, *104*, 9540−9553.
(59) Gouterman, M. Spectra of Porphyrins. *J. Mol. Spectrosc.* **1961**, *6*, 138−163.
(60) Gouterman, M.; Wagniere, G. H. Spectra of Porphyrins. Part II. Four Orbital Model. *J. Mol. Spectrosc.* **1963**, *11*, 108−127.
(61) Weiss, C. In *The Porphyrins*; Dolphin, D., Eds.; Academic Press: New York, 1978; Vol. *III*, pp 211−223.
(62) Kobayashi, M.; Akiyama, M.; Kano, H.; Kise, H. In *Chlorophylls and Bacteriochlorophylls: Biochemistry, Biophysics, Functions and Applications*; Grimm, B., Porra, R. J., Rüdiger, W., Scheer, H., Eds.; Springer: Dordrecht, The Netherlands, 2006; Vol. *25*, pp 79−94.
(63) Novoderezhkin, V.; Marin, A.; van Grondelle, R. Intra- and Inter-Monomeric Transfers in the Light Harvesting LHCII Complex: the Redfield-Förster Picture. *Phys. Chem. Chem. Phys.* **2011**, *13*, 17093−17103.
(64) Müh, F.; Madjet, M. E.-A.; Renger, T. Structure-Based Identification of Energy Sinks in Plant Light-Harvesting Complex II. *J. Phys. Chem. B* **2010**, *114*, 13517−13535.

DOI: 10.1021/acs.jpcb.7b02021
J. Phys. Chem. B 2017, 121, 5331−5339